Biliverdin Reductase A is a major determinant of neuroprotective Nrf2 signaling

Chirag Vasavda[a,1], Ruchita Kothari[a,1], Navneet Ammal Kaidery[b,c], Suwarna Chakraborty[d], Sunil Jamuna Tripathi[d], Ryan S. Dhindsa[e,f,g], Samaneh Saberi[h], Julia E. Lefler[h], Priyanka Kothari[i], Kalyani Chaubey[j,k,l,m], Adele M. Snowman[a], Michael C. Ostrowski[h], Eugenio Barone[n], Lakshminarayan M. Iyer[o], L. Aravind[o], Sudarshana M. Sharma[h], Andrew A. Pieper[j,k,l,m,p,q], Bobby Thomas[b,c,r,s], Solomon H. Snyder[a,d,t,2], Bindu D. Paul[a,d,t,u,2]

[a]The Solomon H. Snyder Department of Neuroscience, Johns Hopkins University School of Medicine, Baltimore, MD, USA.
[b]Darby Children's Research Institute, Medical University of South Carolina, Charleston, SC, USA.
[c]Department of Pediatrics, Medical University of South Carolina, Charleston, SC, USA.
[d]Department of Pharmacology and Molecular Sciences, Johns Hopkins University School of Medicine, Baltimore, MD, USA.
[e]Department of Pathology and Immunology, Baylor College of Medicine, Houston, TX, USA
[f]Jan and Dan Duncan Neurological Research Institute, Texas Children's Hospital, Houston, TX, USA.
[g]Department of Molecular and Human Genetics, Baylor College of Medicine, Houston, TX, USA.
[h]Department of Biochemistry and Molecular Biology and Hollings Cancer Center, Medical University of South Carolina, Charleston, SC, USA.
[i]Department of Cell Biology, Johns Hopkins University School of Medicine, Baltimore, MD, USA.
[j]Department of Psychiatry, Case Western Reserve University School of Medicine, Cleveland, OH, USA
[k]Brain Health Medicines Center, Harrington Discovery Institute, University Hospitals Cleveland Medical Center, Cleveland, OH, USA.
[l]Department of Pathology, Case Western Reserve University, School of Medicine, Cleveland, OH, USA.
[m]Department of Neuroscience, Case Western Reserve University, School of Medicine, Cleveland, OH, USA.
[n]Department of Biochemical Sciences "A. Rossi-Fanelli", Sapienza University of Rome, Rome, Italy.
[o]Computational Biology Branch, Division of Intramural Research, National Library of Medicine, National Institutes of Health, Bethesda, MD, USA.
[p]Geriatric Psychiatry, GRECC, Louis Stokes Cleveland VA Medical Center, Cleveland, OH, USA.
[q]Institute for Transformative Molecular Medicine, School of Medicine, Case Western Reserve University, Cleveland, OH, USA.
[r]Department of Neuroscience, Medical University of South Carolina, Charleston, SC, USA.
[s]Department of Drug Discovery, Medical University of South Carolina, Charleston, SC, USA.
[t]Department of Psychiatry and Behavioral Sciences, Johns Hopkins University School of Medicine, Baltimore, MD, USA.
[u]Lieber Institute for Brain Development, Baltimore, MD, USA.
[1]These authors contributed equally.

[2]Correspondence to

Bindu D. Paul, Solomon H. Snyder

Email: bpaul8@jhmi.edu; ssnyder@jhmi.edu

Author Contributions: CV, RK, AAP, BT, SHS and BDP designed the study. CV, RT, NAK, SC, SJT, PK, KC, SS, JL, JEL, NAM, AMS, MCO, EB, LMI, LA, AAP, BT, SHS and BDP conducted experiments and/or analysis. NAK, SS, JL, SMS, MCO and BT collaborated on the ChIP-seq

analysis. LMI and LA collaborated on the phylogenetic and sequence of analysis of BVR and HO proteins. BT, AAP, SHS, and BDP provided resources and funding. CV, RT, LMI, LA, BT, AAP, SHS, and BDP wrote the paper with input from all authors.

Competing Interest Statement: The authors do not have any competing interests.

Keywords: Biliverdin reductase A, oxidative stress, Nrf2 signaling, neuroprotection, gene regulation

Abstract

Biliverdin reductase A (BVRA), the terminal enzyme in heme catabolism, generates the neuroprotective and lipophilic antioxidant bilirubin. Here, we identify a novel non-enzymatic role for BVRA in redox regulation. We show that BVRA directly interacts with nuclear factor erythroid-derived factor-like 2 (Nrf2), the master regulator of redox homeostasis, to modulate target signaling pathways. ChIP-seq and RNA-seq analyses reveal that this interaction coordinates the expression of neuroprotective genes that are typically dysregulated in Alzheimer's disease and other neurodegenerative conditions. Thus, this previously unknown BVRA-Nrf2 axis controls an essential pathway of redox signaling in neuroprotection. Our findings establish BVRA as a dual-function integrator of antioxidant defenses in both the lipophilic and hydrophilic subcellular compartments, bridging these two distinct and critical cellular protection mechanisms in the brain. This advancement in understanding the endogenous antioxidant system of the brain positions the BVRA-Nrf2 axis as a promising therapeutic target for neurodegenerative disease.

Significance Statement

We show a non-canonical role for biliverdin reductase A (BVRA), classically known as the biosynthetic enzyme for bilirubin, in nonenzymatic modulation of antioxidant neuroprotective nuclear factor erythroid-derived factor-like 2 (Nrf2) signaling in the brain. Both BVRA and Nrf2 signaling are compromised in neurodegenerative diseases such as Alzheimer's disease, and the BVRA-Nrf2 axis offers a new direction for developing neuroprotective therapies.

Main Text

Introduction

Biliverdin reductase A (BVRA), encoded by the *Blvra* gene, and the terminal enzyme in heme catabolism and the major biosynthetic enzyme for bilirubin in adults (Fig. 1*A*) (1, 2). Bilirubin is a potent lipophilic antioxidant with protective efficacy in advanced cardiovascular disease associated with hyperbilirubinemia (3-9), as well as in malaria (10) and metabolic disorders (11, 12). Beyond its canonical role, BVRA exhibits additional diverse enzymatic and non-enzymatic functions, modulating key signaling pathways such as focal adhesion kinase signaling in the brain, insulin signaling, phosphoinositide 3-kinase (PI3K)/Protein kinase B (Akt) signaling, and mitogen-activated protein kinase (MAPK) cascades (11, 13-21). Interestingly, at near-neutral pH BVRA utilizes NADH as a cofactor, whereas it uses NADPH at alkaline pH, enabling flexibility of function under different cellular conditions (22-24). Importantly, while BVRA's roles in peripheral tissues are well-documented, its functions in the central nervous system are not as well understood, despite its significant expression in brain (2).

We previously showed that both bilirubin and BVRA are highly abundant in the lipid-rich brain (2). Bilirubin, being lipophilic, functions in a manner complementary to glutathione (GSH), the abundant hydrophilic antioxidant to confer beneficial effects (2, 7-9, 25). Bilirubin more effectively prevents lipid peroxidation than soluble cellular components, such as protecting cytosolic proteins from oxidation (2, 8). Bilirubin is also a potent scavenger of superoxide ($O_2^{\bullet-}$) radicals, with mice lacking BVRA displaying elevated susceptibility to oxidative stress (2, 9). We have shown that bilirubin is a potent scavenger of $O_2^{\bullet-}$ and cannot neutralize other forms of reactive oxygen species (ROS) such as H_2O_2 and the hydroxyl radical ($OH^{\bullet}$)(2).

Despite bilirubin's apparent lack of reactivity towards these ROS, *Blvra*$^{-/-}$ mice are still hypersensitive to H_2O_2 and complementing cells with BVRA is protective, suggesting that these mice may be deficient in a mechanism dependent on BVRA, but not bilirubin to counteract oxidative stress (2). Here, we reveal a redox-regulatory role of BVRA that entails a non-enzymatic interaction with the nuclear factor erythroid-derived factor-like 2 (Nrf2) transcription factor, which is well known as the master regulator of antioxidant responses (26). We demonstrate that direct binding of BVRA to Nrf2 enhances transcriptional regulation of neuroprotective gene networks implicated in Alzheimer's disease (AD) and neurodegeneration. This BVRA-Nrf2 axis establishes a novel link between heme metabolism and physiologic redox homeostasis, revealing opportunities to therapeutically bolster endogenous neuroprotection.

Results

Heme-independent expression patterns and functional roles of brain BVRA

The first enzyme in heme catabolism in the brain, heme oxygenase 2 (HO-2) accounts for most of the HO activity in the nervous system and, like HO-1, regulates redox balance (27, 28). HO-2 deletion aggravates oxidative stress induced by seizures, glutamate, and inflammation, and also causes cerebral vascular injury (29). To determine whether BVRA operates independently of the heme oxygenase (HO) system, we first identified brain cell types in which heme metabolism is crucial. Using single-cell RNA sequencing (scRNA-seq), we compared *Blvra* (which encodes BVRA) and *Hmox2* (which encodes HO-2) expression profiles in whole-brain lysates. Both *Blvra* and *Hmox2* were detected in numerous cell types in the brain (Fig. 1*B*). On the other hand, *Hmox1* mRNA (which encodes HO-1) is inducible (30) and not expressed at baseline, rendering it undetectable in most cells analyzed. Notably, *Blvra* exhibited more restricted cellular expression than *Hmox2*, with HO-2 mRNA levels nearly tripling those of *Blvra* transcripts. Strikingly, 23% of brain cells expressed *Blvra* mRNA without detectable *Hmox2* mRNA and only 10% expressed both *Blvra* and *Hmox2* (Fig. 1*C*), a pattern observed broadly across cell types and brain regions (Fig. 1*D*). This surprisingly broad presence of BVRA in the absence of HO-2, is puzzling and suggests

a potential function independent of heme metabolism. This dissociation, corroborated by independent datasets (Allen Brain Atlas, Protein Atlas) (31), implies that BVRA operates in contexts unrelated to bilirubin generation.

We next examined the evolutionary histories of these principal enzymes involved in heme degradation: the BVRs (BVRA, BVRB), and HO. BVRA and BVRB are distinct enzymes with BVRA being the main bilirubin producing enzyme in adults and BVRB in the fetal stages (32). BVRA belongs to the expansive glyceraldehyde 3-phosphate dehydrogenase (GAPDH)-like clade of redox enzymes, whose members feature an N-terminal NADPH/NADH-binding Rossmann fold catalytic domain and a C-terminal GADC domain responsible for substrate selection and binding. Structural studies of the related *Synechocystis* BVRA revealed that its C-terminal domain accommodates two biliverdin molecules via π-π stacking, both of which are believed to participate in the redox reaction. Based on the *Synechocystis* BVRA structure and its interactions with NADPH and biliverdin, and the sequence conservation pattern, we identified several residues for further mutational studies (G17, E97, R172, R46, R227, K219). We also noticed a cysteine residue (C292) that is conserved across vertebrates and some cyanobacteria, which may play a role in BVRA-mediated redox homeostasis (Fig. S1). In contrast, BVRB lacks the GADC domain and is comprised of only the NADPH-binding Rossmann fold catalytic domain, which is also present in BVRA (Fig. 1*F*). Consistent with the absence of a dedicated substrate-binding domain, it exhibits greater substrate promiscuity. HO, on the other hand, is a heme-dependent all–α-helical oxygenase that is structurally unrelated to BVRA and BVRB.

Given that homologs of these enzymes are reported in prokaryotes, we explored their phylogenetic affinities and genomic contexts to gain insights into the evolution of this pathway. Phylogenetic analyses show that both BVRA and HO are ultimately of cyanobacterial origin. However, their patterns of acquisition by eukaryotes differ, with the gene for BVRA appearing to have been transferred from cyanobacteria to an early metazoan (Fig. 1*E*) and HO having been acquired earlier in eukaryotic evolution, as evidenced by its presence in diverse eukaryotic lineages such as oomycetes and haptophytes. BVRB, by contrast, appears to represent a lateral transfer from a firmicute lineage again into an early metazoan. Notably, homologs related to all three enzymes were transferred on multiple independent occasions from prokaryotes to eukaryotes. For example, one such paralog of BVRA in eukaryotes, the diphenol detoxifying enzyme dihydrodiol dehydrogenase (DHDH), was independently acquired from bacteria.

Furthermore, even within metazoans, the phyletic patterns of BVRA and BVRB enzymes differ considerably: for example, BVRB is widely present in insects, where HO and BVRA are largely absent. However, HO and BVRA, display a degree of concordance in their distribution among other metazoans. These patterns support the hypothesis that the heme catabolic pathway combining the roles of BVRA and HO likely evolved near the base of the animal lineage, whereas BVRB, given its broader substrate range, including flavins and ferric ions, may have been secondarily

incorporated into heme catabolism in vertebrates, perhaps as an extension of its more generalized role in redox modification of exogenous toxic small molecules. The cyanobacterial versions of HO and BVRA likely functioned originally in the metabolism of phycobilins associated with proteins of their light-harvesting systems. Their early incorporation and shared distribution in animals imply that they were co-opted for the emerging importance of heme metabolism in the context of oxygen transport in multicellular animals.

To further characterize the potentially novel function of BVRA decoupled from HO, we utilized *Blvra*$^{-/-}$ mice lacking exon 3 (encoding the NAD(P)H-binding domain) abolishing bilirubin production (2). Despite originally creating this model to interrogate bilirubin's antioxidant effects, our earliest observations implicated BVRA itself in redox regulation, including protection against the hydrophilic H_2O_2 oxidant. We therefore generated a series of mutants in the NADPH and biliverdin binding domains of BVRA, including the G17A mutant described earlier (21, 33) to assess their roles in BVRA function (Fig. S1). As previously reported, a glycine to alanine mutation of residue 17 (G17A) disrupted NADPH binding and significantly diminished BVRA-mediated bilirubin production (Fig. 1*G*). Specifically, G17A conferred a 5-fold reduction in Vmax and a 300-fold increase in Km (Fig. 1*H*) of the enzyme. Furthermore, several other mutants derived from residues that are predicted to bind NADPH/NADH or biliverdin also showed diminished activities (Fig. 1*G*).

Next, we transfected BVRA$^{-/-}$ mouse embryonic fibroblasts (MEFs) with WT or G17A-BVRA to test whether this enzymatically dead mutant could rescue cells exposed to H_2O_2 despite its inability to produce bilirubin (Fig. 1*I*). G17A-BVRA rescues *Blvra*$^{-/-}$ cells to a similar extent as WT-BVRA, hinting further at a redox function of BVRA independent of bilirubin production and heme catabolism (Fig. 1*J*).

Depleting BVRA blunts Nrf2 signaling

To assess how BVR may exert antioxidant activity independent of its role in bilirubin production, we monitored the gene expression of several antioxidant genes via unbiased whole transcriptome sequencing of WT and BVRA$^{-/-}$ hippocampal neurons at baseline and under oxidative stress induced by H_2O_2. After this toxic exposure, several genes were differentially expressed in both cell types (Fig. 2*A-C,* (*SI Data Table 1*). We focused on genes that show a fold difference of at least 2 in upregulation or downregulation between the WT and *Blvra*$^{-/-}$ genotypes. Among the genes upregulated, the cholesterol biosynthetic pathway was most prominently represented, with upregulation in BVRA$^{-/-}$ cells under stress BVRA$^{-/-}$ cells. Most significant among the downregulated pathways was the nuclear factor erythroid-derived factor-like 2 (Nrf2) signaling pathway (Fig. 2*D,* right panel), with Nrf2 ranking significantly high amongst the transcription factors implicated in the differential gene expression between the WT and BVRA$^{-/-}$ cells (Fig. 2*E*). We therefore chose to focus on Nrf2 signaling for the remainder of our study to determine the specific role of BVRA in the response to oxidative stress.

Nrf2 is a transcription factor that regulates the expression of several antioxidant response proteins. Under basal conditions, Nrf2 is sequestered by the Kelch-like ECH-associated protein 1 (Keap1) in the cytosol and ubiquitinated for targeted degradation by the 26S proteasome(34). In response to oxidative stress, Keap1 is modified on its reactive cysteine residues and dissociates from Nrf2, preventing its ubiquitination and proteasomal degradation (35-39). Nrf2 then translocates to the nucleus, where it binds the antioxidant response element (ARE) to orchestrate transcription of a battery of vital antioxidant genes necessary for cytoprotection. To evaluate whether Nrf2 signaling is disrupted in BVRA$^{-/-}$ cells, we analyzed the transcript levels of Nrf2 target genes such as *Hmox1, Gclc*, *Gsta2* and *Cxcl2* (Fig. 2*F-I*). The expression of *Hmox1*, *Gclc* (which encodes the catalytic subunit of glutamate–cysteine ligase, a key enzyme in glutathione biosynthesis) and *Gsta2* (which encodes glutathione S-transferase A2, an enzyme involved in detoxification of electrophilic compounds) were blunted in the BVRA$^{-/-}$ cells, whereas the proteins involved in the immune response and inflammation such as *Cxcl2* (encoding the chemokine (C-X-C motif) ligand 2) were upregulated.

Next, we compared the activity of the Nrf2 promoter in WT and BVRA$^{-/-}$ cells using a luciferase reporter assay. In this dual-luciferase firefly reporter system, where the luciferase gene is regulated by the promoter for glutathione S-transferase A4 (GSTA4), a target of Nrf2. Thus, Nrf2 activity at the *Gsta4* promoter initiates luciferase transcription, which can be measured via luciferin luminescence. We quantified the activation of the *Gsta4* promoter in WT and BVRA$^{-/-}$ MEFs in response to three Nrf2 activators: H_2O_2, sulforaphane (SFN), and tert-butyl hydroquinone (*t*-BHQ). SFN is a compound known to modify the reactive cysteines on Keap1, thus releasing Nrf2 before ubiquitination and increasing overall expression of intracellular Nrf2 (40). *t*-BHQ is also known to activate Nrf2, although its mechanism not well-established (41). H_2O_2 treatment increases luciferin reporter detection in WT cells, indicating Nrf2 activation by proxy of GST gene transcription. However, this increase is not seen in BVRA$^{-/-}$ cells, which are unable to elicit Nrf2 activity and GST luciferase expression. The same pattern was also noted in the SFN and tBHQ treatment conditions (Fig. 2*J*).

To determine whether enzymatically dead BVRA also potentiates Nrf2 transcriptional activity, we introduced WT and G17A BVRA in a HEK293 cell line harboring an Nrf2 regulated luciferase reporter. In this HEK293 cell line, the promoter controlling luciferase expression is directly downstream of the antioxidant response element promoter that Nrf2 binds, allowing us to use luciferase expression as a readout for Nrf2 transcriptional activity in general and not limited to GSTA4 expression as in the previous experiment. WT- and G17A-BVRA both increase luciferase activity significantly and to the same degree in each treatment condition (Fig. 2*K*). Enzymatically dead BVRA was equally efficacious as WT BVRA in activating Nrf2 *in vitro*, underscoring BVRA's novel non-catalytic Nrf2-inducing role. We next analyzed the effect of erastin, an inhibitor of the cystine transporter, one of whose subunits is encoded by *Slc7a11*, a target of Nrf2, on the viability

of these cells. BVRA$^{-/-}$ MEFs were more susceptible to increasing concentrations of erastin as compared to WT cells, further confirming that depletion of BVRA compromises Nrf2 signaling (Fig. 2*L*).

BVRA physically and genetically interacts with Nrf2

To characterize the relationship between BVRA and Nrf2, we aimed to breed BVRA and Nrf2 double-knockout mice. In our attempts to create such mice, no *Blvra*$^{-/-}$/ *Nfe2l2*$^{-/-}$ pups were ever obtained, indicating that this interaction is crucial for survival and function. In the crosses conducted, we expected roughly 9% of the pups to present with the double-null genotype but were unable to obtain double knockout pups (Fig. 3*A, B*). All other possible genotypes were generated at near their expected frequencies. This finding suggests that BVRA and Nrf2 are genetically linked and that deleting both genes is embryonic lethal, confirming a genetic interaction between *Blvra* and *Nfe2l2* that is crucial for survival.

To determine whether BVRA interacts with Nrf2, we conducted a GST pull down assay in HEK293 transfected with constructs harboring GFP-tagged Nrf2 and either GST vector alone or a construct encoding GST-BVRA. GST-BVRA robustly bound Nrf2 unlike GST alone, as revealed by western blot analysis (Fig. 3*C*). Given that BVRA and BVRB are the two enzymes involved in bilirubin production, but have completely different evolutionary histories and are only remotely related, we analyzed whether BVRB has an Nrf2-interacting role. We simultaneously co-expressing GFP-Nrf2 with either GST-BVRB, GST-BVRA or GST alone in HEK293 cells and conducted GST pulldown assays. We observed that BVRB does not associate with Nrf2 and this function of BVR remains specific to BVRA (Fig. 3*D*). To determine whether this interaction is dependent on the BVRA's bilirubin-producing activity, we transfected cells with Nrf2 and enzymatically dead G17A BVRA, which cannot bind the cofactors NADPH or NADH. G17A BVRA not only pulls down Nrf2 but does so more robustly than WT BVRA, indicating that this interaction is independent of its catalytic function (Fig. 3*E*).

As both BVRA and Nrf2 modulate redox homeostasis, we also analyzed whether the formation of the BVRA-Nrf2 complex increases in response to oxidative stress. We therefore simulated pro-oxidant conditions to monitor changes in the BVR-Nrf2 interaction. HEK293 cells exposed to H_2O_2 and pyrogallol, a superoxide generator (42), exhibit increased Nrf2 expression compared to vehicle conditions, which was associated with increased BVRA-Nrf2 complex formation via co-immunoprecipitation. (Fig. 3*F*). Notably, there was no affinity difference in interaction under different redox conditions.

We also analyzed whether BVRA influences stability of Nrf2. As Nrf2 stability and levels are regulated by ubiquitination, we first examined whether BVRA increases Nrf2 expression by binding and hindering ubiquitin association. Through co-immunoprecipitation, we find that BVRA does not bind or associate with ubiquitin (Fig. S2A). Additionally, we observed no changes in levels

of Nrf2 in the presence or absence of BVRA both under basal conditions or in response to H_2O_2, sulforaphane or *t*-BHQ exposure (Fig. S2B). Next, we monitored Nrf2 levels in the nucleus of WT and BVRA$^{-/-}$ cells upon induction of oxidative stress or with treatment with Nrf2 activators such as sulforaphane. While whole cell levels of Nrf2 are higher in WT cells with oxidative stress compared to cells lacking BVRA, the levels of Nrf2 in the nucleus are similar in both WT and BVRA$^{-/-}$ MEFs under the conditions analyzed (Fig. S3C).

Lastly, we investigated whether binding of BVRA to Nrf2 is modulated by its substrate, biliverdin. We transfected HEK293 cells with GFP-Nrf2 and either GST-BVRA or GST vector, treated cells with biliverdin and conducted a pulldown assay. In the presence of biliverdin, interaction of BVRA with Nrf2 decreased as compared to cells which were not treated (Fig. 3*G*). Thus it appears that the presence of substrates for BVRA can influence its non-canonical functions.

BVRA is a component of the transcriptional program of Nrf2-regulated promoters *in vivo*

BVRA has been reported to be a transcription factor regulating the expression of activating transcription factor 2 (ATF2) and HO-1 by binding to the AP-1 sites in their promoters (43, 44). Considering the physical and genetic interaction of Nrf2 and BVRA, we examined whether BVRA might potentially coregulate Nrf2 target genes. We performed a genome-wide ChIP-seq analysis of MEFs generated from previously described FLAG-BVRA transgenic mouse line (21) using FLAG and Nrf2 antibodies (Fig. 4*A-D*). The peak distribution demonstrated that approximately 10 % of the peaks were located in promoter regions with majority (approximately 40%) harbored in distal intergenic regions (10 to 50kb; Fig. 4*B*). Motif analysis of both FLAG-BVRA and Nrf2 ChIP-seq peaks identified bZIP motifs such as Bach1::Mafk motif and Nrf2 motif respectively (Fig. 4*B*). ChIP-seq peaks were annotated by nearest neighbor method to identify genes that both Nrf2 and BVRA potentially regulate. Approximately 43% of the genes in the annotated ChIP-seq data had both BVRA and Nrf2 peaks (*SI Data Table 2*). We further overlaid the BVRA-Nrf2 gene set with RNAseq-data from WT and BVRA$^{-/-}$ cells. K-means clustering of the Nrf2-BVRA gene expression identified two clusters that are predominantly enriched for pathways that are dysregulated in neurodegenerative diseases (Fig. S3). Further, Gene Set Enrichment Analysis (GSEA) analysis of BVR-Nrf2 associated genes revealed inflammatory pathways, heme metabolism and redox signaling (Fig. 4*E*).

Thus, interaction of BVRA with Nrf2 is physiologically relevant and fits in well with the observation that this association is increased in response to oxidative stress to increase the transcription of Nrf2 targets to maintain redox balance in cells

Discussion

In this study, we show that BVRA, the biosynthetic enzyme for bilirubin, is an essential regulator of neuroprotective signaling by the master regulator of redox homeostasis, Nrf2. We showed previously that bilirubin is a potent antioxidant capable of scavenging superoxide (2). However, the role of BVRA in oxidative stress independent of its catalytic activity has not been explored (2). Using advanced genomic techniques, as well as evolutionary, mutational, genetic, and biochemical studies, we examined the non-canonical role of BVRA in the antioxidant stress response. sc-RNA-seq analysis of the brain revealed that a significant proportion of brain cell populations expressed BVRA but not HO-2, the precursor to BVRA in heme catabolism in the brain, indicating additional functions for BVRA distinct from its classical role in bilirubin production. Phylogenetic analysis revealed that although HO-2 and BVRA originated in the cyanobacteria in the context of phycobilisome synthesis in the light-harvesting complex, they were acquired at different points in time in the eukaryotes. Thus, they were co-opted and combined in a common heme catabolism pathway only in Metazoa. Using sequence conservation information from a multiple sequence alignment, we mutated key residues in BVRA and tested these mutants for BVRA activity. Further, the presence of a single exposed conserved cysteine within a CC motif at the extreme C-terminus in vertebrates suggests that this residue might be involved in the sensing of the redox status of the cell.

Amongst the mutants generated, the G17A mutant was severely compromised in the ability to produce bilirubin as this mutation affects its ability to bind the cofactor, NAD(P)H as reported earlier (21, 33). Interestingly, G17A BVRA rescued H_2O_2-mediated cell death, demonstrating a protective role of BVRA, distinct from its catalytic activity. Furthermore, unbiased RNA-seq analysis of hippocampal neurons derived from BVRA$^{-/-}$ mice, identified Nrf2 signaling as a top downregulated pathway. In support of these findings, both WT and G17A BVRA bind Nrf2 and stimulate transcription of target genes. We also noted that in the presence of biliverdin, the substrate for production of bilirubin, the binding of BVRA to Nrf2 is diminished. This suggests a dual yet distinct role of BVRA with its additional ability to regulate redox metabolism via Nrf2. Although BVRA does not influence the nuclear translocation of Nrf2, it is essential for optimal function of Nrf2 as revealed by our RNA-seq and ChIP-seq data. This role of BVRA as a regulator that interacts with a transcription factor is closely paralleled by another catalytically inactive Rossman fold oxidoreductase harboring a from the same clade as BVRA, Gal80, which has been co-opted as a regulator that binds transcription factors (45).

Our studies revealed that multiple pathways are co-regulated by the BVRA-Nrf2-bound genes, which encompass a range of functions, including mitochondrial function, heme metabolism to cytokine signaling and oxidative stress response. Delineating this function of BVRA allows us to understand heme metabolism in the context of oxidant-induced aging and disease. While heme oxygenases, which catalyze the first step of heme degradation, are known targets for redox regulation, their overexpression leads to deleterious off-target effects including inflammation and

cognitive decline (46) reducing its therapeutic efficacy (47). Likewise, while bilirubin itself acts as an endogenous and exogenous ROS suppressor, its effects are limited to distinct forms of ROS (2). While exogenous bilirubin may only be effective in curtailing excess $O_2^{\bullet-}$, activators of BVRA expression may be able to regulate ROS in a more all-encompassing manner. The BVRA/Nrf2 interaction is relevant to a wide array of ROS-mediated pathologies. Suboptimal Nrf2 activity has been observed in neurodegenerative diseases such as PD and AD (48, 49). However, currently known activators of Nrf2 are predominantly electrophilic compounds that exert adverse side effects. In such a scenario, molecules that activate BVRA expression or stimulate its transcriptional activity are of significant therapeutic value. BVRA's role in activating Nrf2 provides a new therapeutic signaling pathway that mitigates a broader array of oxidative species via multiple downstream effectors. Augmenting BVRA therefore promises to a more reliable and efficacious approach for diseases involving imbalanced Nrf2 activity. Additionally, modulating the Nrf2 pathway through BVRA may also mitigate ferroptosis, an iron-mediated form of cell death, which is observed in several neurodegenerative diseases as both BVRA and Nrf2 regulate iron disposition, through its metabolism or transport, and loss of either of these proteins result in accumulation of excess iron and vulnerability to oxidative stress (50-53).

Collectively, our findings reveal a previously unrecognized and crucial function of BVRA, which bridges two distinct and critical pathways, namely heme metabolism and Nrf2 signaling, to afford cytoprotective effects. Furthermore, BVRA orchestrates antioxidant stress responses in both the lipophilic and hydrophilic subcellular compartments of the cell through not only the production of bilirubin which directly scavenges $O_2^{\bullet-}$radicals, but also through its role as a transcriptional regulator, respectively (Fig. 4*F*). Augmenting this latter pathway may offer therapeutic benefits in diseases characterized by redox imbalance. Both the enzymatic and non-enzymatic roles of BVRA participate in diverse aspects of normal physiology, and characterizing these activities and their cell-type-specific roles will likely reveal new paradigms for treating neurodegenerative diseases.

Materials and Methods

Plasmids/cDNA

Plasmids encoding GST-BVR (GST-BVRA) and GST-BVRB were generated by cloning cDNA encoding human BVRA and BVRB into pCMV-GST vector (Clontech/TaKaRa). Likewise, the myc-BVRA (myc-BVRA) plasmid was generated by cloning cDNA of human BLVRA into pCMV-myc vector. The GFP-Nrf2 plasmid was generated by cloning cDNA of Nrf2 into GFP-vector.

Cell Culture

Mouse Embryonic Fibroblasts (MEFs)

WT, BVRA$^{-/-}$, and Flag BVRA MEFs were isolated as previously described (2). In brief, embryonic day 14.5 (E14.5) embryos were obtained from timed BVRA$^{+/-}$ matings. The pups were decapitated and eviscerated, after which the remaining portion was trypsinized and sheared. Isolated MEFs were plated in 2 wells of a 6-well plate and cultured overnight in DMEM (Gibco) supplemented with 10% FBS, 100 U/mL penicillin and streptomycin, and 2 mM glutamine at 37°C with 5% CO_2. MEFs were then expanded to 6-well plates and transiently transfected with SV40T antigen (Addgene) and maintained until stably proliferative. DNA was isolated from the heads of the pups and genotyped to confirm the genotype of the corresponding MEF cell line. Data for WT and BVRA$^{-/-}$ cells were drawn from experiments on at least two independent cell lines of each genotype.

Human Embryonic Kidney (HEK) 293 Cells

HEK293 cells were obtained from the American Type Culture Collection. HEK293 cells were cultured in Dulbecco's Modified Eagle Medium (DMEM), 10% fetal bovine serum, penicillin/streptomycin (100 U/ml), and glutamine (2 mM) in an atmosphere of 5% CO_2 at 37°C.

Primary neurons

Primary WT and BVRA$^{-/-}$ neurons were isolated as previously described (2). In brief, hippocampi from embryonic day 18 (E18) embryos were isolated and washed with HBSS. Tissue was then incubated with 0.25% trypsin in HBSS for 18 min at 37°C in a conical tube, after which trypsin was inactivated with the addition of FBS. Tissue were then pelleted at 2000*g* for 5 min at 25°C, after which the supernatant trypsin/FBS was aspirated off. Tissue were then rinsed twice with HBSS, resuspended in HBSS, and then gently triturated through a fire-polished glass pipette to promote additional dissociation. Tissue was then filtered through a 70 µm nylon cell strainer to remove debris. The dissociated cells were pelleted at 2000*g* for 5 min at 25°C and then resuspended in neuronal culture media (composed of Neurobasal (Gibco) supplemented with 2% B-27 supplement and 2 mM glutamine). Cells were filtered once more through a 70 µm nylon cell strainer. Dissociated cells were then plated onto rinsed, poly-D-lysine-coated dishes. Four days later, the conditioned media was supplemented with fresh neuronal culture media. The day before dissections, plates were prepared and coated in 0.25 mg/mL poly-D-lysine overnight at 37°C. Just prior to plating, plates were rinsed three times with sterile water and once with neuronal culture media.

Transfection

HEK293 cells were transfected with Lipofectamine 3000 (ThermoFisher) as per the manufacturer's instructions. Briefly, HEK293 cells were seeded in either 10 cm dishes ($3x10^6$ cells) or in 60 mm dishes ($1x10^6$ cells). The next day, transfection complexes were added dropwise to the plated cells. For cells in 10 cm dishes, 25 µg of DNA, 23.7 µL of Lipofectamine, and 50 µL of P3000 were brought to a volume of 1 mL in serum-free Optimem media (Thermo). For cells in 60 mm dishes, 5

ug of DNA, 8.25 µL Lipofectamine, and 10 µL P300 were brought to a volume of 500 µL in Optimem. Cells were harvested 48 hours after transfection.

Additional details of reagents and methods are available in the *Supplementary Section.*

Acknowledgments

BDP, SHS and AAP were supported by the American Heart Association and Paul Allen Foundation Initiative in Brain Health and Cognitive Impairment (19PABH134580006). BDP and AAP by NIH/NIA 1R01AG071512. BDP also acknowledges support from NIH/NIA 1R21AG073684, NIH NIDA, grant P50 DA044123, funding from the Solve-ME foundation and the Catalyst Award from Johns Hopkins University. B.T. was supported by NIH AG077396, NS101967, NS133688, and the Department of Defense HT94252310443. M.C.O. and S.M.S. were supported by NIH P01CA236778. AAP was supported by The Valour Foundation, as the Rebecca E. Barchas, MD, Professor in Translational Psychiatry of Case Western Reserve University and the Morley-Mather Chair in Neuropsychiatry of University Hospitals of Cleveland Medical Center, and by the Wick Foundation, Department of Veterans Affairs Merit Award I01BX005976, NIH/NIA RO1AGs066707, NIH/NIA 1 U01 AG073323, the Louis Stokes VA Medical Center resources and facilities, the Lincoln Neurotherapeutics Research Fund, the Leonard Krieger Fund of the Cleveland Foundation, the Meisel & Pesses Family Foundation, and an anonymous donor. LMI and LA are supported by the funds of the Division of Intramural Research of the National Library of Medicine at the National Institutes of Health. We also acknowledge biorender.com, a service we used to design our schematic figures and graphical abstract, and Intelligenomica LLC for genomics support.

References

1. Paul BD & Pieper AA (2024) Neuroprotective Roles of the Biliverdin Reductase-A/Bilirubin Axis in the Brain. *Biomolecules* 14(2).
2. Vasavda C*, et al.* (2019) Bilirubin Links Heme Metabolism to Neuroprotection by Scavenging Superoxide. *Cell Chem Biol* 26(10):1450-1460 e1457.
3. Vitek L*, et al.* (2002) Gilbert syndrome and ischemic heart disease: a protective effect of elevated bilirubin levels. *Atherosclerosis* 160(2):449-456.
4. Woronyczova J*, et al.* (2022) Serum Bilirubin Concentrations and the Prevalence of Gilbert Syndrome in Elite Athletes. *Sports Med Open* 8(1):84.
5. Schwertner HA, Jackson WG, & Tolan G (1994) Association of low serum concentration of bilirubin with increased risk of coronary artery disease. *Clin Chem* 40(1):18-23.
6. Djousse L*, et al.* (2001) Total serum bilirubin and risk of cardiovascular disease in the Framingham offspring study. *Am J Cardiol* 87(10):1196-1200; A1194, 1197.
7. Stocker R, Yamamoto Y, McDonagh AF, Glazer AN, & Ames BN (1987) Bilirubin is an antioxidant of possible physiological importance. *Science* 235(4792):1043-1046.
8. Sedlak TW*, et al.* (2009) Bilirubin and glutathione have complementary antioxidant and cytoprotective roles. *Proc Natl Acad Sci U S A* 106(13):5171-5176.

9. Vasavda C, Snyder SH, & Paul BD (2021) Quantitative measurement of reactive oxygen species in ex vivo mouse brain slices. *STAR Protoc* 2(1):100332.
10. Figueiredo A*, et al.* (2025) A Metabolite-Based Resistance Mechanism Against Malaria. *bioRxiv*.
11. Lanzillotta C*, et al.* (2024) Biliverdin Reductase-A integrates insulin signaling with mitochondrial metabolism through phosphorylation of GSK3beta. *Redox Biol* 73:103221.
12. Cimini FA*, et al.* (2019) Reduced biliverdin reductase-A levels are associated with early alterations of insulin signaling in obesity. *Biochim Biophys Acta Mol Basis Dis* 1865(6):1490-1501.
13. Cimini FA, Perluigi M, Barchetta I, Cavallo MG, & Barone E (2022) Role of Biliverdin Reductase A in the Regulation of Insulin Signaling in Metabolic and Neurodegenerative Diseases: An Update. *Int J Mol Sci* 23(10).
14. Kapitulnik J & Maines MD (2009) Pleiotropic functions of biliverdin reductase: cellular signaling and generation of cytoprotective and cytotoxic bilirubin. *Trends Pharmacol Sci* 30(3):129-137.
15. Salim M, Brown-Kipphut BA, & Maines MD (2001) Human biliverdin reductase is autophosphorylated, and phosphorylation is required for bilirubin formation. *J Biol Chem* 276(14):10929-10934.
16. Lerner-Marmarosh N*, et al.* (2005) Human biliverdin reductase: a member of the insulin receptor substrate family with serine/threonine/tyrosine kinase activity. *Proc Natl Acad Sci U S A* 102(20):7109-7114.
17. Wegiel B*, et al.* (2009) Cell surface biliverdin reductase mediates biliverdin-induced anti-inflammatory effects via phosphatidylinositol 3-kinase and Akt. *J Biol Chem* 284(32):21369-21378.
18. Hinds TD, Jr.*, et al.* (2016) Biliverdin Reductase A Attenuates Hepatic Steatosis by Inhibition of Glycogen Synthase Kinase (GSK) 3beta Phosphorylation of Serine 73 of Peroxisome Proliferator-activated Receptor (PPAR) alpha. *J Biol Chem* 291(48):25179-25191.
19. Stec DE*, et al.* (2020) Biliverdin Reductase A (BVRA) Knockout in Adipocytes Induces Hypertrophy and Reduces Mitochondria in White Fat of Obese Mice. *Biomolecules* 10(3).
20. Chen W*, et al.* (2021) Bilirubin deficiency renders mice susceptible to hepatic steatosis in the absence of insulin resistance. *Redox Biol* 47:102152.
21. Vasavda C*, et al.* (2022) Biliverdin reductase bridges focal adhesion kinase to Src to modulate synaptic signaling. *Sci Signal* 15(733):eabh3066.
22. Kutty RK & Maines MD (1981) Purification and characterization of biliverdin reductase from rat liver. *J Biol Chem* 256(8):3956-3962.
23. Maines MD & Trakshel GM (1993) Purification and characterization of human biliverdin reductase. *Arch Biochem Biophys* 300(1):320-326.
24. Maines MD, Mayer RD, Erturk E, Huang TJ, & Disantagnese A (1999) The oxidoreductase, biliverdin reductase, is induced in human renal carcinoma--pH and cofactor-specific increase in activity. *J Urol* 162(4):1467-1472.
25. Dore S*, et al.* (1999) Bilirubin, formed by activation of heme oxygenase-2, protects neurons against oxidative stress injury. *Proc Natl Acad Sci U S A* 96(5):2445-2450.
26. Baird L & Dinkova-Kostova AT (2011) The cytoprotective role of the Keap1-Nrf2 pathway. *Arch Toxicol* 85(4):241-272.
27. Verma A, Hirsch DJ, Glatt CE, Ronnett GV, & Snyder SH (1993) Carbon monoxide: a putative neural messenger. *Science* 259(5093):381-384.
28. Dore S*, et al.* (2000) Heme oxygenase-2 acts to prevent neuronal death in brain cultures and following transient cerebral ischemia. *Neuroscience* 99(4):587-592.
29. Parfenova H & Leffler CW (2008) Cerebroprotective functions of HO-2. *Curr Pharm Des* 14(5):443-453.
30. Maines MD, Trakshel GM, & Kutty RK (1986) Characterization of two constitutive forms of rat liver microsomal heme oxygenase. Only one molecular species of the enzyme is inducible. *J Biol Chem* 261(1):411-419.
31. Zhang Y*, et al.* (2018) Bliverdin reductase-A improves neurological function in a germinal matrix hemorrhage rat model. *Neurobiol Dis* 110:122-132.

32. O'Brien L, Hosick PA, John K, Stec DE, & Hinds TD, Jr. (2015) Biliverdin reductase isozymes in metabolism. *Trends Endocrinol Metab* 26(4):212-220.
33. Lerner-Marmarosh N, Miralem T, Gibbs PE, & Maines MD (2007) Regulation of TNF-alpha-activated PKC-zeta signaling by the human biliverdin reductase: identification of activating and inhibitory domains of the reductase. *FASEB J* 21(14):3949-3962.
34. Itoh K*, et al.* (1999) Keap1 represses nuclear activation of antioxidant responsive elements by Nrf2 through binding to the amino-terminal Neh2 domain. *Genes Dev* 13(1):76-86.
35. Baird L & Yamamoto M (2020) The Molecular Mechanisms Regulating the KEAP1-NRF2 Pathway. *Mol Cell Biol* 40(13).
36. Dinkova-Kostova AT, Kostov RV, & Canning P (2017) Keap1, the cysteine-based mammalian intracellular sensor for electrophiles and oxidants. *Arch Biochem Biophys* 617:84-93.
37. Uruno A & Motohashi H (2011) The Keap1-Nrf2 system as an in vivo sensor for electrophiles. *Nitric Oxide* 25(2):153-160.
38. Kobayashi A*, et al.* (2006) Oxidative and electrophilic stresses activate Nrf2 through inhibition of ubiquitination activity of Keap1. *Mol Cell Biol* 26(1):221-229.
39. Yamamoto M, Kensler TW, & Motohashi H (2018) The KEAP1-NRF2 System: a Thiol-Based Sensor-Effector Apparatus for Maintaining Redox Homeostasis. *Physiol Rev* 98(3):1169-1203.
40. Hu C, Eggler AL, Mesecar AD, & van Breemen RB (2011) Modification of keap1 cysteine residues by sulforaphane. *Chem Res Toxicol* 24(4):515-521.
41. Imhoff BR & Hansen JM (2010) Tert-butylhydroquinone induces mitochondrial oxidative stress causing Nrf2 activation. *Cell Biol Toxicol* 26(6):541-551.
42. Yin XJ, Ma JY, Antonini JM, Castranova V, & Ma JK (2004) Roles of reactive oxygen species and heme oxygenase-1 in modulation of alveolar macrophage-mediated pulmonary immune responses to Listeria monocytogenes by diesel exhaust particles. *Toxicol Sci* 82(1):143-153.
43. Ahmad Z, Salim M, & Maines MD (2002) Human biliverdin reductase is a leucine zipper-like DNA-binding protein and functions in transcriptional activation of heme oxygenase-1 by oxidative stress. *J Biol Chem* 277(11):9226-9232.
44. Kravets A, Hu Z, Miralem T, Torno MD, & Maines MD (2004) Biliverdin reductase, a novel regulator for induction of activating transcription factor-2 and heme oxygenase-1. *J Biol Chem* 279(19):19916-19923.
45. Aravind L & Koonin EV (1998) Eukaryotic transcription regulators derive from ancient enzymatic domains. *Curr Biol* 8(4):R111-113.
46. Wang D*, et al.* (2015) Overexpression of heme oxygenase 1 causes cognitive decline and affects pathways for tauopathy in mice. *J Alzheimers Dis* 43(2):519-534.
47. Uttara B, Singh AV, Zamboni P, & Mahajan RT (2009) Oxidative stress and neurodegenerative diseases: a review of upstream and downstream antioxidant therapeutic options. *Curr Neuropharmacol* 7(1):65-74.
48. Wang Q*, et al.* (2017) Meta-Analysis of Parkinson's Disease and Alzheimer's Disease Revealed Commonly Impaired Pathways and Dysregulation of NRF2-Dependent Genes. *J Alzheimers Dis* 56(4):1525-1539.
49. Soni P, Sharma SM, Pieper AA, Paul BD, & Thomas B (2025) Nrf2/Bach1 signaling axis: A promising multifaceted therapeutic strategy for Alzheimer's disease. *Neurotherapeutics* 22(3):e00586.
50. Stockwell BR (2022) Ferroptosis turns 10: Emerging mechanisms, physiological functions, and therapeutic applications. *Cell* 185(14):2401-2421.
51. Mezzanotte M & Stanga S (2024) Brain Iron Dyshomeostasis and Ferroptosis in Alzheimer's Disease Pathophysiology: Two Faces of the Same Coin. *Aging Dis*.
52. Berndt C*, et al.* (2024) Ferroptosis in health and disease. *Redox Biol* 75:103211.
53. Wang ZL, Yuan L, Li W, & Li JY (2022) Ferroptosis in Parkinson's disease: glia-neuron crosstalk. *Trends Mol Med* 28(4):258-269.
54. Pereira PJ*, et al.* (2001) Structure of human biliverdin IXbeta reductase, an early fetal bilirubin IXbeta producing enzyme. *Nat Struct Biol* 8(3):215-220.

Figure Legends

Fig. 1. BVRA exhibits expression profiles and redox homeostatic activity unlinked to heme catabolism. (*A*) Schematic representation of the heme catabolic pathway. Heme derived from hemoglobin from senescent red blood cells is metabolized by heme oxygenases (HO) to produce the green pigment, biliverdin. Biliverdin reductase A (BVRA) then reduces biliverdin to produce the yellow pigment, bilirubin, which is a potent antioxidant. (*B*) T-distributed stochastic neighbor embedding (t-SNE) analysis of single-cell RNA expression in primary neuronal cultures from WT C57BL/6J mice. Each point represents a single cell. Left panel: Cells are clustered by gene expression into populations with similar cell type and function. Right panel: Expression distribution of *Blvra*, *Hmox2*, both individually and together, across cell population clusters. (*C*) Quantified percentage of total cells expressing *Blvra*, *Hmox2,* and a combination of both genes. (*D*) Scaled Pearson residuals of *Blvra* and *Hmox2* gene expression in different cell populations. A residual >1 indicates a higher observed to expected frequency ratio. Each point represents a single cell. (*E*) Phylogenetic trees of BVRA, HO, and BVRB respectively. (*F*) Protein structures of BVRA and BVRB obtained from Kavanagh et. al. (PDB Entry - 2H63 (pdb_00002h63) and Periera et. al., respectively (54). Structural comparison of the two BVR proteins aligned at the Rossmann fold of the NADPH-binding domain. (*G*) Activity of WT BVRA and BVRA mutants measured at varying concentrations of NADPH and 10 μM biliverdin. Activity measured by absorbance reading of bilirubin production at 442 nM with V_o calculated according to the method by Michaelis and Menten. n = 3 in triplicate. (*H*) Quantified V_{max} and K_m of WT BVRA and BVRA mutants. (*I*) Viability of WT and BVRA MEFs transfected with empty vector, WT BVRA, and G17A- BVRA after 8 h of exposure to serial dosing of H_2O_2. Data is normalized to viability of vehicle condition. (*J*) Quantified LD_{50}s (I) of H_2O_2 exposure in WT and BVRA MEFS. n = 3 in triplicate.

Fig.2. Nrf2 activity is disrupted in BVRA$^{-/-}$ neurons and fibroblasts

(*A*) Volcano plot analysis of genes from WT and *Blvra*$^{-/-}$ primary hippocampal neurons. Each plot displays the fold change of gene expression on a log scale with their corresponding P values plotted on a log scale. Each dot represents a gene of interest. Change in gene expression between WT from vehicle to H_2O_2 condition are shown (*B*) Change in gene expression in *Blvra*$^{-/-}$ neurons from vehicle to H_2O_2 condition. (*C*) Change in gene expression between WT and *Blvra*$^{-/-}$ neurons after H_2O_2 treatment. Red dots indicate genes that are upregulated with H_2O_2 condition in *Blvra*$^{-/-}$ neurons. Blue dots indicate genes that are downregulated with H_2O_2 condition in *Blvra*$^{-/-}$ neurons. (*D*) Logarithmically-scaled *p* values of molecular pathways that are upregulated (left panel) and downregulated (right panel) in *Blvra*$^{-/-}$ neurons compared to WT controls under the H_2O_2 condition. (*E*) Transcription factors ranked by log-scaled *p* values. A higher *p* value indicates transcription

factors that are more significantly dysregulated in BVRA$^{-/-}$ compared to WT neurons in the H_2O_2 condition. Transcription factors ranked from 1, most significant, to 1279, least significant. (*F-I*) Validation of expression of genes regulated by Nrf2 in WT and BVRA$^{-/-}$ neurons. Wild-type (WT) and BVRA$^{-/-}$ primary hippocampal neurons were treated with or without 200 μM H_2O_2 for 6 h and expression of Nrf2 targets were analyzed by qPCR. n=3, SEM, p <0.01, Student's t test. (*J*) Luciferase reporter assays in WT and BVRA$^{-/-}$ MEFs transfected with Gsta4 luciferase reporter construct after exposure to vehicle, 50 μM H_2O_2, 10 μM SFN, and 25 μM TBHQ. n = 4 in triplicate. Sidak's multiple comparison (*K*) Luciferase reporter assays in stable cell HEK293 cell lines harboring a 5xARE reporter constructs transfected with either WT BVRA or G17A- BVRA and after exposure to either vehicle, 200 μM H_2O_2, 10 μM SFN, and 25 μM TBHQ. n = 4 in triplicate. Tukey's multiple comparison. (*L*) BVRA$^{-/-}$ MEFs are more sensitive to erastin, an inhibitor of the XcT transporter. WT and BVRA$^{-/-}$ MEFs were treated overnight for 18 hours with increasing concentrations of erastin, a xCT inhibitor and ferroptosis inducer, and cell viability was assessed by MTT assay. n=7, SEM, $^{*}p < 0.05$, $^{**}p < 0.01$, $^{***}p < 0.001$, Student's t test.

Fig. 3. BVRA genetically and physically interacts with Nrf2

(*A*) Expected versus observed frequency of pups from the *Blvra*$^{-/-}$ and *Nfe2l2*$^{-/-}$ (*Nrf2*$^{-/-}$) cross. (*B*) Number of observed pups of each genotype. n = 114 pups total. (*C*) GST pulldown with glutathione sepharose beads of GST-BVRA and GFP-Nrf2 transfected HEK293 cells. GST-only vector control was used as a negative control. Blots were probed for GFP-Nrf2 and GST-BVRA with their respective tags. (*D*) Co-immunoprecipitation of GFP-Nrf2 with GST- BVRA and GST-BVRB. Inputs at the right indicate samples taken before incubation in beads to monitor whole cell expression of transfected proteins. Blots were probed for GFP-NRF2 and GST-BVRA with their respective tags. (*E*) GFP-Nrf2 co-immunoprecipitation with GST-WT BVRA and GST-G17A-BVRA. Shorter exposure was used for G17A IP lanes and longer exposure was used for the remaining lanes. Blots were probed for GFP-Nrf2 and GST-BVR with their respective tags. (*F*) Co-immunoprecipitation of GST-BVRA and GFP-Nrf2 with varying oxidative stress conditions, including vehicle, 200 μM H_2O_2, and 100 μM pyrogallol. Blots were probed for GFP-Nrf2 and GST-BVRA with their respective tags. (*G*) Interaction of GST-BVRA and GFP-Nrf2 in the presence of 10 μM biliverdin in HEK293 cells. Blots were probed for GFP-Nrf2 and GST-BVRA with their respective tags.

Fig. 4. ChIP-Seq analysis reveals genes regulated by both BVRA and Nrf2. (*A*) Schematic representation of methods used for genomic analysis. (The data obtained from ChIP-seq was overlaid onto the RNA-seq data from the primary hippocampal neurons in vehicle treated (V) or H_2O_2-treated conditions (T) (*B*) Global representation of Flag-BVRA and Nrf2 peak distribution and Motifs. (*C*) Venn diagram showing overlap of genes associated with both BVRA and Nrf2 peaks.

(*D*) MA plot showing differentially expressed readcounts between WT and BVRA$^{-/-}$. (E) GSEA analysis of BVRA-Nrf2 associated genes from C. (*F*) Summary of canonical and non-canonical roles of BVRA. BVRA acts on heme-derived biliverdin to produce the antioxidant-cytoprotectant bilirubin, which scavenges superoxide generated from mitochondrial activity and other processes to maintain redox balance. In addition to this role in heme catabolism, BVR also functions as a serine-threonine and tyrosine kinase that modulates several signaling pathways. We show here that BVRA also regulates Nrf2 signaling, independent of its enzymatic roles.

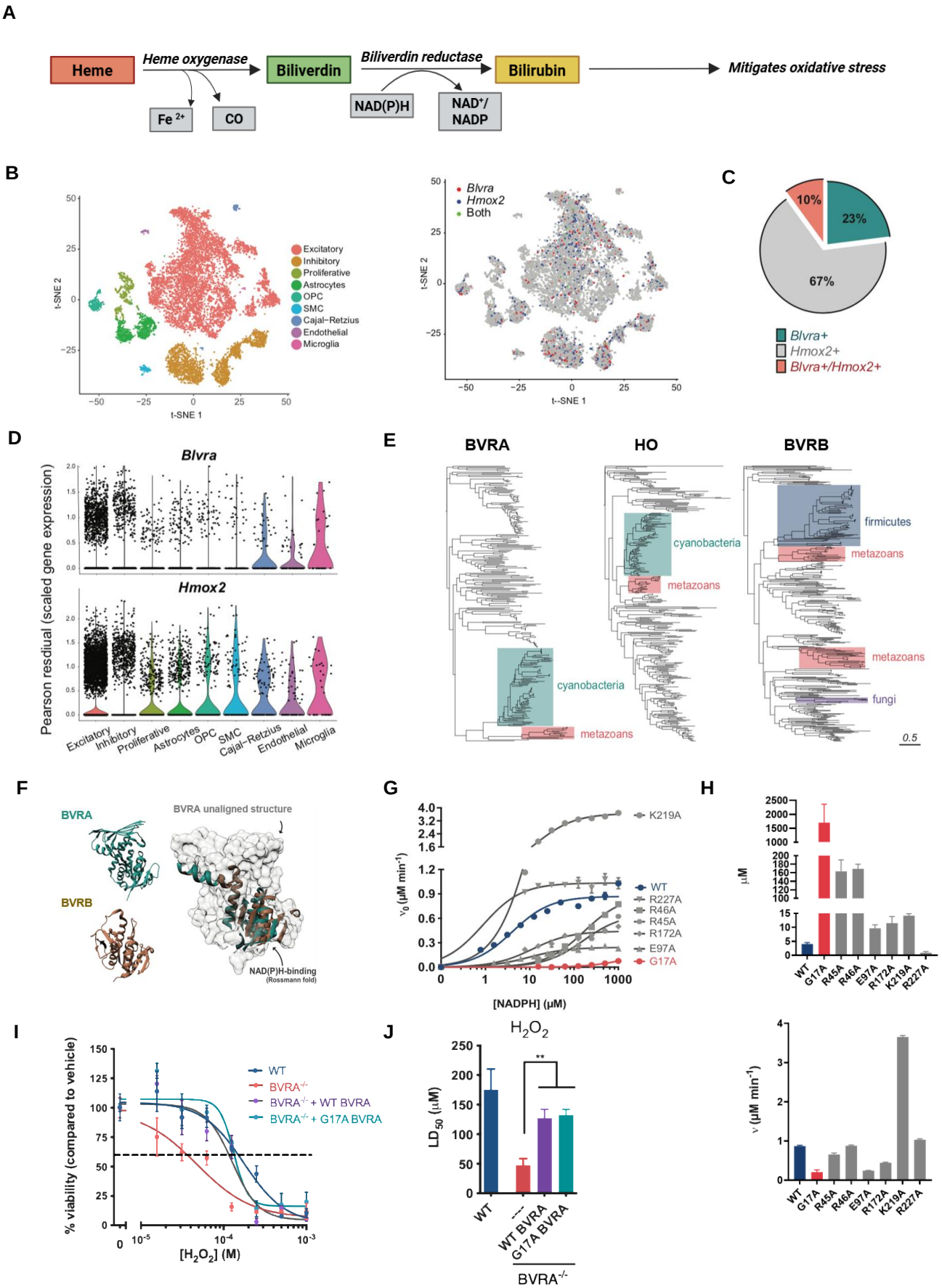
A
Heme
Heme oxygenase
Fe 2+
CO
Biliverdin
Biliverdin reductase
NAD(P)H
NAD+/ NADP
Bilirubin
Mitigates oxidative stress
B
Excitatory
Inhibitory
Proliferative
Astrocytes
OPC
SMC
Cajal–Retzius
Endothelial
Microglia
t-SNE 1
t-SNE 2
Blvra
Hmox2
Both
C
10%
23%
67%
Blvra+
Hmox2+
Blvra+/Hmox2+
D
Blvra
Hmox2
Pearson residual (scaled gene expression)
Excitatory
Inhibitory
Proliferative
Astrocytes
OPC
SMC
Cajal–Retzius
Endothelial
Microglia
E
BVRA
HO
BVRB
cyanobacteria
metazoans
firmicutes
fungi
0.5
F
BVRA
BVRB
BVRA unaligned structure
NAD(P)H-binding
(Rossmann fold)
G
K219A
WT
R227A
R46A
R45A
R172A
E97A
G17A
[NADPH] (μM)
H
μM
WT
G17A
R45A
R46A
E97A
R172A
K219A
R227A
I
WT
BVRA-/-
BVRA-/- + WT BVRA
BVRA-/- + G17A BVRA
% viability (compared to vehicle)
[H2O2] (M)
J
H2O2
LD50 (μM)
WT

WT BVRA
G17A BVRA
BVRA-/-
v (μM min-1)

Figure 1

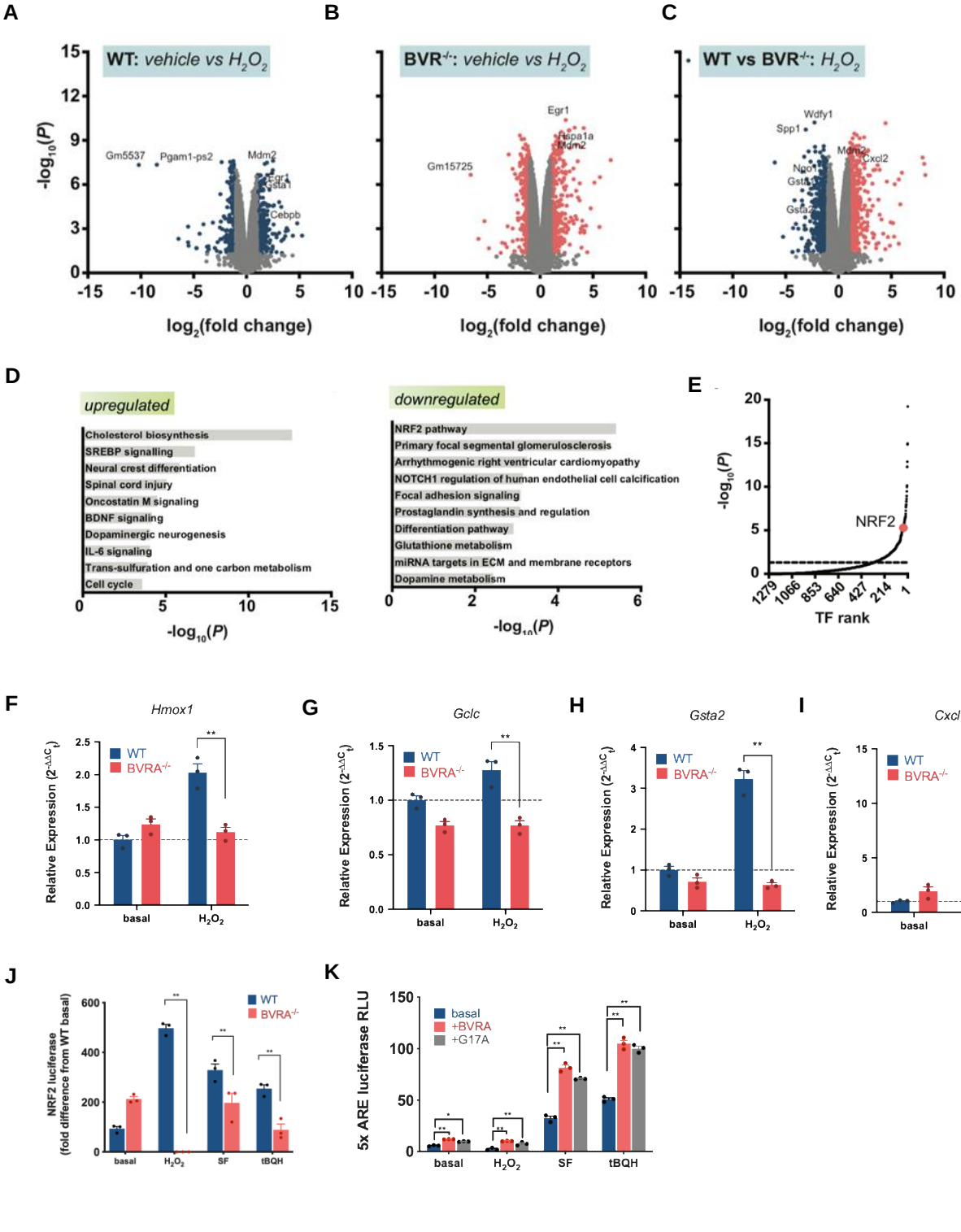
A
WT: vehicle vs H2O2
Gm5537
Pgam1-ps2
Mdm2
Egr1
Gsta1
Cebpb
-log10(P)
log2(fold change)
B
BVR-/-: vehicle vs H2O2
Egr1
Hspa1a
Mdm2
Gm15725
log2(fold change)
C
WT vs BVR-/-: H2O2
Wdfy1
Spp1
Mdm2
Cxcl2
Nqo1
Gsta1
Gsta2
log2(fold change)
D
upregulated
Cholesterol biosynthesis
SREBP signalling
Neural crest differentiation
Spinal cord injury
Oncostatin M signaling
BDNF signaling
Dopaminergic neurogenesis
IL-6 signaling
Trans-sulfuration and one carbon metabolism
Cell cycle
-log10(P)
downregulated
NRF2 pathway
Primary focal segmental glomerulosclerosis
Arrhythmogenic right ventricular cardiomyopathy
NOTCH1 regulation of human endothelial cell calcification
Focal adhesion signaling
Prostaglandin synthesis and regulation
Differentiation pathway
Glutathione metabolism
miRNA targets in ECM and membrane receptors
Dopamine metabolism
-log10(P)
E
-log10(P)
NRF2
TF rank
F
Hmox1
Relative Expression (2-ΔΔCt)
WT
BVRA-/-
basal
H2O2
G
Gclc
H
Gsta2
I
Cxcl2
J
NRF2 luciferase (fold difference from WT basal)
SF
tBQH
K
5x ARE luciferase RLU
basal
+BVRA
+G17A

Figure 2

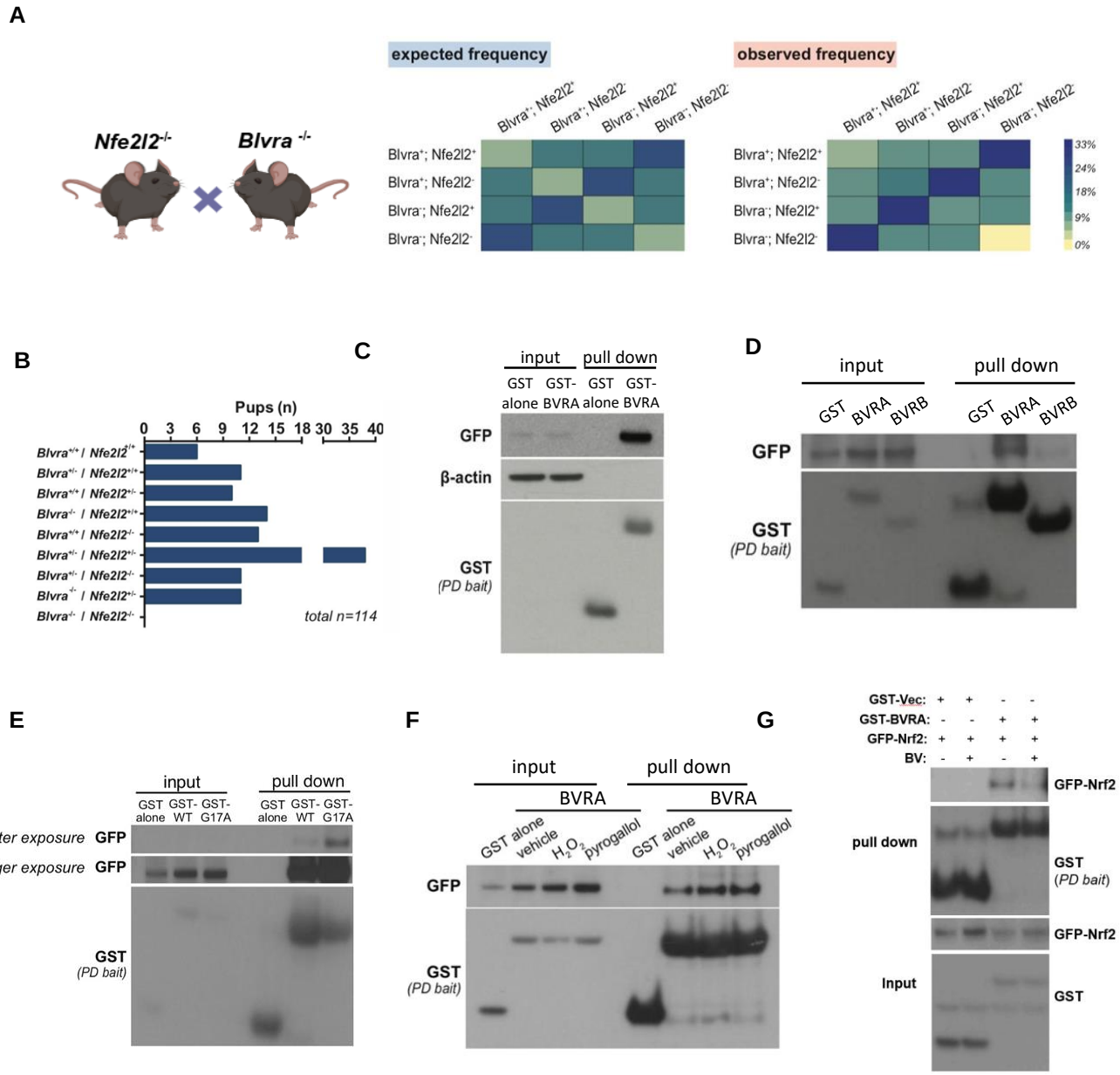
A
Nfe2l2-/-
Blvra -/-
expected frequency
observed frequency
Blvra+; Nfe2l2+
Blvra+; Nfe2l2-
Blvra-; Nfe2l2+
Blvra-; Nfe2l2-
33%
24%
18%
9%
0%
B
Pups (n)
0 3 6 9 12 15 18 30 35 40
total n=114
C
input
pull down
GST alone
GST-BVRA
GFP
β-actin
GST (PD bait)
D
input
pull down
GST
BVRA
BVRB
GFP
GST (PD bait)
E
input
pull down
GST alone
GST-WT
GST-G17A
shorter exposure
longer exposure
GFP
GST (PD bait)
F
input
pull down
BVRA
GST alone
vehicle
H2O2
pyrogallol
GFP
GST (PD bait)
G
GST-Vec:
GST-BVRA:
GFP-Nrf2:
BV:
GFP-Nrf2
pull down
GST (PD bait)
Input
GST

Figure 3

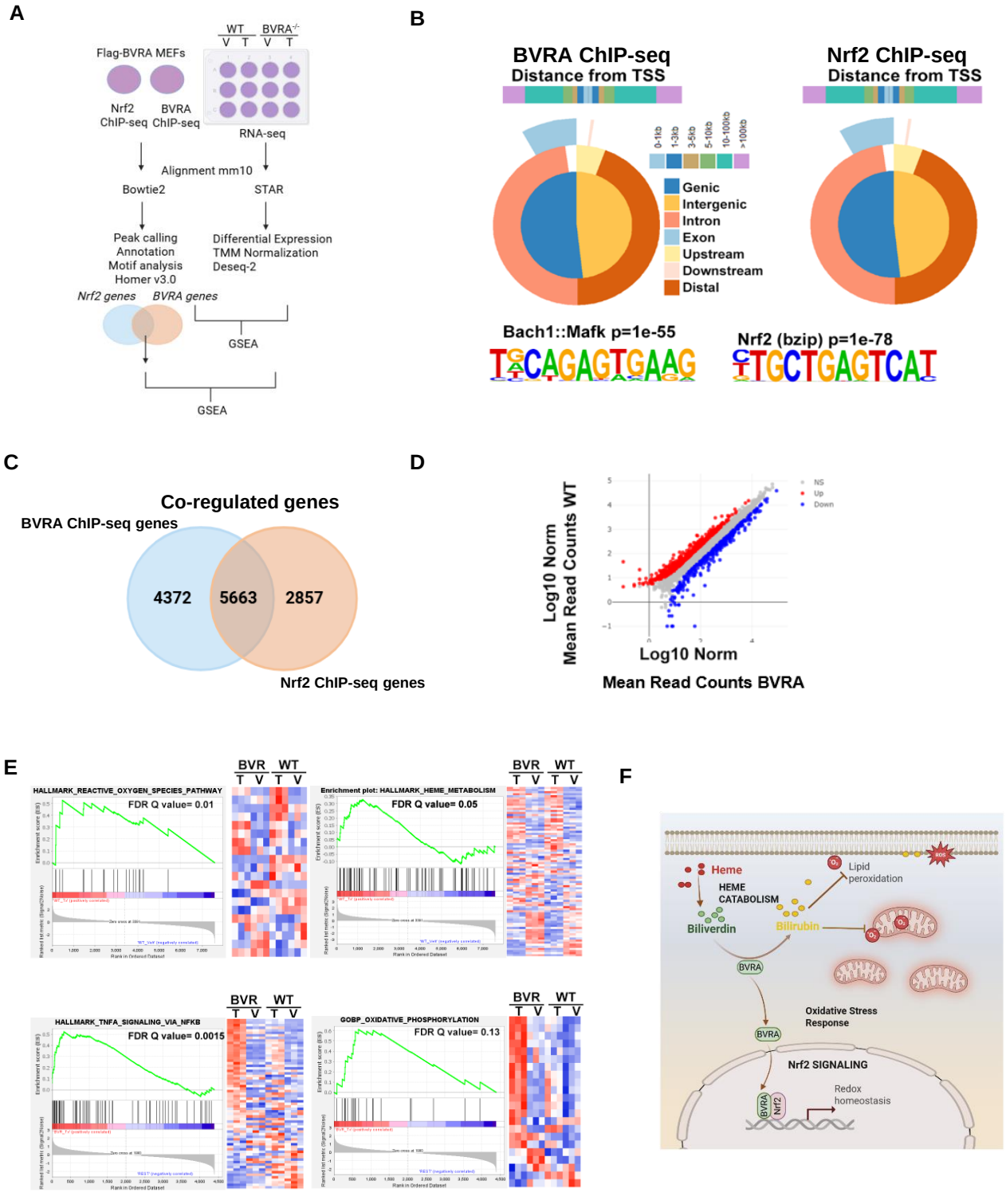
A
WT
BVRA-/-
V T V T
Flag-BVRA MEFs
Nrf2 ChIP-seq
BVRA ChIP-seq
RNA-seq
Alignment mm10
Bowtie2
STAR
Peak calling
Annotation
Motif analysis
Homer v3.0
Differential Expression
TMM Normalization
Deseq-2
Nrf2 genes
BVRA genes
GSEA
GSEA
B
BVRA ChIP-seq
Distance from TSS
Nrf2 ChIP-seq
Distance from TSS
0-1kb
1-3kb
3-5kb
5-10kb
10-100kb
>100kb
Genic
Intergenic
Intron
Exon
Upstream
Downstream
Distal
Bach1::Mafk p=1e-55
Nrf2 (bzip) p=1e-78
C
Co-regulated genes
BVRA ChIP-seq genes
4372
5663
2857
Nrf2 ChIP-seq genes
D
Log10 Norm
Mean Read Counts WT
Log10 Norm
Mean Read Counts BVRA
NS
Up
Down
E
BVR WT
T V T V
HALLMARK_REACTIVE_OXYGEN_SPECIES_PATHWAY
FDR Q value= 0.01
Enrichment plot: HALLMARK_HEME_METABOLISM
FDR Q value= 0.05
HALLMARK_TNFA_SIGNALING_VIA_NFKB
FDR Q value= 0.0015
GOBP_OXIDATIVE_PHOSPHORYLATION
FDR Q value= 0.13
F
Heme
HEME
CATABOLISM
Biliverdin
Bilirubin
Lipid
peroxidation
ROS
BVRA
Oxidative Stress
Response
Nrf2 SIGNALING
Nrf2
Redox
homeostasis

Figure 4

Supplementary Information
Biliverdin Reductase A is a major determinant of neuroprotective Nrf2 signaling

Chirag Vasavda[a,1], Ruchita Kothari[a,1], Navneet Ammal Kaidery[b,c], Suwarna Chakraborty[d], Sunil Jamuna Tripathi[d], Ryan S. Dhindsa[e,f,g], Samaneh Saberi[h], Julia E. Lefler[h], Priyanka Kothari[i], Kalyani Chaubey[j,k,l,m], Adele M. Snowman[a], Michael C. Ostrowski[h], Eugenio Barone[n], Lakshminarayan M. Iyer[o], L. Aravind[o], Sudarshana M. Sharma[h], Andrew A. Pieper[j,k,l,m,p,q], Bobby Thomas[b,c,r,s], Solomon H. Snyder[a,d,t,2], Bindu D. Paul[a,d,t,u,2]

*Solomon H. Snyder; *Bindu D. Paul
Email: ssnyder@jhmi.edu
bpaul8@jhmi.edu

Supporting Information Text

Materials and Methods

Western Blotting

For western blot analysis, tissues were dounce homogenized at 4°C in lysis buffer (pH 7.4 solution of 50 mM Tris-HCl, 150 mM NaCl, 0.1% SDS, 0.5% sodium deoxycholate, and 1% Triton X-100) supplemented with protease inhibitors (Sigma). Lysates were then pulse sonicated and centrifuged at 16,000*g* for 15 min at 4°C. Fifteen micrograms of cleared lysate were run on a 4-12% polyacrylamide Bis-Tris gradient gel in running buffer (pH 7.3 solution of 50 mM MES, 50 mM Tris Base, 0.1% SDS, 1 mM EDTA) and then transferred to a PVDF membrane. Membranes were blocked with 5% milk in TBS-T (pH 7.6 solution of 16 mM Tris-HCl, 140 mM NaCl, 0.1% Tween-20) and incubated with primary antibodies in 3% bovine serum albumin (BSA) (w/v) overnight at 4°C. The following day, membranes were washed with TBS-T, and then incubated with secondary antibodies in 3% BSA for 1 h at 25°C. The following primary antibodies were used: rabbit anti-BVRA (Abcam ab180208; 1:1,000), rabbit anti-Nrf2 (Abcam ab62352; 1:1,000), rabbit anti-Nrf2 (Santa Cruz sc-722; 1:1,000), rabbit anti-GFP (Cell Signaling 2956; 1:1,000), mouse anti-GST (Abcam ab3416 1:20,000), mouse anti-myc (Abcam ab9106; 1:10,000), and mouse anti-β-actin (Santa Cruz sc-47778 HRP; 1:10,000). The following secondary antibodies were used: sheep anti-mouse IgG (GE Healthcare NA931; 1:10,000), and donkey anti-rabbit IgG (GE Healthcare NA934; 1:10,000).

Subcellular Fractionation

Cells were lysed in membrane prep buffer (10 mM Hepes pH 7.4, containing 1 mM EGTA, 1 mM dithiothreitol, 10% sucrose) supplemented with protease inhibitors (Sigma). After lysis cells were snap-frozen in liquid nitrogen and then thawed briefly in a cold-water bath, and then kept on ice thereafter. A 30G needle was then used to lyse cells 3-4 times. The cell homogenate was then filtered through a nylon mesh (pore size 75 μm) to remove any intact cells. 100μL of this sample was collected and set aside for the whole cell fraction. The remainder of the sample was centrifuged at 1,000 *g* for 10 minutes at 4°C. The supernatant was collected and set aside as the cytosolic fraction. The pellet was then re-homogenized in membrane buffer and spun down once again at 1,000 *g* for 10 minutes at 4°C. The pellet was then washed once more in membrane buffer by pipetting buffer over the pellet without homogenizing it. The cells were then centrifuged one last time at 1,000 g for 10 minutes at 4°C, and the supernatant was discarded. The pellet was re-homogenized as the nuclear fraction. The previously collected cytosolic fraction was then centrifuged at 11,000*g* for 20 minutes at 4°C and the pellet was discarded. All whole cell, cytosolic, and nuclear fractions were then pulse-sonicated to shear DNA and spun down at 16,000 *g* for 15 minutes at 4°C. The fractions were then processed for immunoblot analysis.

BVRA enzymatic activity assays

BVRA activity was assayed at pH 8.5 at 37°C. 250 nM of purified WT and mutant BVRA were separately incubated for 5 min at room temperature in a pH 8.5 solution of 50 mM Tris, NADP+, glucose-6-phosphate, and glucose-6-phosphate dehydrogenase (NADPH Regeneration System, Promega v9510). The samples were then placed at 37°C and spiked with varying concentrations of biliverdin IXα (250 nM to 20 uM). Reaction rates were determined by monitoring the change in absorbance at 442 nm over time. Enzyme activity was determined by the Michaelis and Menten (Michaelis Menten 1913). In brief, the absorbance of bilirubin was monitored over time for each concentration of biliverdin. The slope of each curve in the linear range was recorded and plotted against the corresponding substrate concentration. This data was then fit to the Michaelis-Menten equation to determine the K_m and V_{max} of the enzyme-substrate reaction (1).

Methylthiazoletetrazolium (MTT) assays

WT and BVRA$^{-/-}$ MEFs were plated at a density of 75,000 cells/well in a 24-well plate. After 24h, BVRA$^{-/-}$ cells were transfected with empty vector, WT-BVRA, and G17A-BVRA respectively. The following day, the culture media was supplemented with varying H_2O_2 concentrations (0 to 250uM) for 6 hours, after which the media was replaced with fresh media containing 0.5 mg/mL MTT for 1 h. The media was then removed before dissolving the reduced cellular MTT in DMSO. Cell viability was determined by measuring the absorbance at 570 nm and normalizing absorbances to the vehicle condition.

Single-Cell RNA Sequencing

Single-cell RNA-sequencing was performed as previously described (2). Briefly, whole brains from postnatal day 0 pups were dissected and dissociated for sequencing. Single cell RNA-seq libraries were constructed using the 10X Chromium Single Cell 3′ Reagent Kits v2 according to manufacturer's descriptions and subsequently sequenced on a NovaSeq 6000. Reads were aligned to the mm10 genome using the 10X CellRanger pipeline with default parameters to generate the feature-barcode matrix. 610 Downstream quality control and analyses on feature-barcode matrices were performed with Seurat v3. Genes that were not detected in at least 4 cells were excluded. Cells with fewer than 1,000 genes or more than 5,000 genes were also excluded from analysis. We also excluded cells in which greater than 15% of reads mapped to mitochondrial genes. The filtered matrices were log-normalized and scaled to 10,000 transcripts per cell. Using the variance-stabilizing transformation in the FindVariableFeatures function, we identified the top 2,000 most variable genes per sample. We then harmonized gene expression across datasets prior to clustering by identifying anchors between samples in each dataset using the 620 FindIntegrationAnchors function and then computing an integrated expression matrix from these

anchors as input to the IntegrateData function. We then linearly regressed the number of UMIs per cell and percentage of mitochondrial reads using the ScaleData function and performed dimensionality reduction using PCA. For each dataset, we selected the top 30 dimensions to compute a cellular distance matrix, which was used to generate a K-nearest neighbor graph. The KNN was used as input to the Louvain Clustering algorithm implemented in the FindClusters function. We chose a resolution parameter of 0.8 for clustering via Louvain. To annotate and merge clusters, we performed differential gene expression analysis on the integrated expression values between each cluster using the default parameters in the FindMarkers function

RNA isolation, reverse transcriptase PCR (RT-PCR), and quantitative-PCR (q-PCR)

RNA isolation and qPCR were performed as previously described (3). In brief, WT and BVRA$^{-/-}$ cells were treated with vehicle or 50 μM H_2O_2 for 8 h. Total cellular or tissue RNA was extracted using the RNeasy Plus Universal Kit (Qiagen) per the manufacturer's instructions. RT-PCR was performed with the SuperScript III One-Step RT-PCR System (Invitrogen), whereas q-PCR was performed with the TaqMan RNA-to-C_t 1-Step Kit (Applied Biosystems).

Immunoprecipitation

HEK cells were co-transfected with the plasmids of interest as indicated above. Two days later, the culture media was supplemented with 10 μM MG-132 (Sigma M744) for 4 h. Cells were then lysed in immunoprecipitation buffer (1% Triton-X100, 50 mM Tris, 150 mM NaCl, 5% glycerol, 25 mM NaF, 1 mM Na_3VO_4) supplemented with protease inhibitors (Sigma) and placed on a shaker at 4°C for 15 min. The lysates were then centrifuged at 16,000*g* for 15 min at 4°C. IP samples were incubated with 1 mg of protein lysate and 40 μL of either Glutathione Sepharose 4B (GE Healthcare) or anti-FLAG M2 (Sigma) beads overnight at 4°C. 5% of each sample was set aside as input prior to addition of beads. The following day, beads were pelleted by centrifugation at 2,500g for 2 min at 4 °C. The supernatant was aspirated, and beads were washed 5 times in immunoprecipitation buffer by centrifugation, aspiration, and resuspension. Proteins were eluted from beads by boiling for 5 min at 100°C in LDS sample buffer (Thermo Fisher) and the eluates analyzed by Western blot as described above.

Nrf2 ARE Luciferase Reporter Assay

Nrf2 activity was monitored with a reporter cell line in which changes in Nrf2 activity are coupled to the expression of firefly luciferase (Nrf2/ARE Luciferase Reporter HEK293 Stable Cell Line). Nrf2 ARE HEK293 cells were infected with lentivirus encoding either empty vector, WT-BVRA, or G17A-BVRA were plated at 125,000 cells/well in a 24-well plate. The following day, cells were treated with 200 μM H_2O_2, 10 μM SFN, and 25 μM TBHQ for 6 h. Cells were then lysed in passive lysis buffer (Promega E1941) supplemented with protease inhibitors (Sigma) and let shake at 4°C for

15 minutes. The lysates were then centrifuged at 16,000 *g* for 15 minutes at 4°C and protein estimated using the BCA assay. 15 µL of lysate was mixed with 5 µL of luciferase assay substrate LARII (Promega) and the amount of light produced was measured using a luminometer for a 10 second integration time with a delay of 2 seconds. The luciferase measurement was normalized to protein and reported normalized to the vehicle condition.

GST Firefly Dual Luciferase Assay

WT and BVRA$^{-/-}$ MEFs were plated in a 24-well plate and transfected with NQO1 or GST ARE firefly luciferase and renilla luciferase. Two d post-transfection, cells were treated with H_2O_2, SFN, and tBHQ for 8 hours. Cells were then lysed in passive lysis buffer (Promega E1941) supplemented with protease inhibitors (Sigma) and let shake at 4°C for 15 minutes. The lysates were then spun down at 16,000*g* for 15 min at 4°C and protein estimated using the BCA assay. 15 µL of lysate was mixed with 5 µL of luciferase assay substrate LARII (Promega) and the amount of light produced was measured using a luminometer for a 10 second integration time with a delay of 2 seconds. Afterwards, 5 µL of Stop&Glo Reagent (Promega) was added and measured for 10 seconds with a delay of 2 s to estimate the amount of Renilla luciferase produced. The Renilla measurement and was used as the protein loading control to normalize the signal given by LARII. Data was normalized to the vehicle condition.

Chromatin immunoprecipitation-sequencing (ChIP-seq)

Chromatin immunoprecipitation (ChIP) assays were performed on cultured FLAG-BVRA mouse embryonic fibroblasts from 10 million cells per IP as described previously (4). The chromatin was immunoprecipitated with 10 µg anti-FLAG-M (Sigma Aldrich), 10 µg anti-Nrf2 (D1Z9C-XP Cell Signaling Rabbit mAB #1271) antibodies. 5 ng of the immunoprecipitated chromatin was used for ChIP-seq library preparation using NEBNext library kit (New England Biolabs) and sequenced in Illumina sequencer (50 million paired end reads per sample). Bowtie2 software (5) was used to map the sequence reads to the mm10 mouse genome. Peak calling and motif analysis were done with HOMER v3 software (6). Global annotation of peaks with respect to TSS and gene body was performed with the R Bioconductor package ChIPseeker (7).

Computational analysis

Homologous sequences of BVRA were retrieved using sequence-profile searches done with the PSI-BLAST program (8) against a curated database of completely sequenced genomes as well as a non-redundant protein database from the National Center for Biotechnology Information clustered down to 50%. Retrieved sequences were aligned with the Kalign2 (9) and MAFFT programs (10). For the MAFFT program alignment, the local-pair algorithm was combined with the following parameters: maxiterate, 3,000; op, 1.5; ep, 0.2. The aligned sequences were then used to perform

phylogenetic maximum likelihood analyses using the FastTREE2 program (11). Cartoon structures were rendered with the Mol*(12) or PyMOL (The PyMOL Molecular Graphics System, Version 1.2r3pre, Schrödinger, LLC) software. Alphafold3(13) was used to model predicted interactions of BVRA with its NADPH, Biliverdin and Nrf2

Statistical Analysis. Results are presented as means ± SEM for at least three independent experiments. The sample sizes used were based on the magnitude of changes and consistency expected. Statistical significance was reported as appropriate. *P* values were calculated with Student's *t* test.

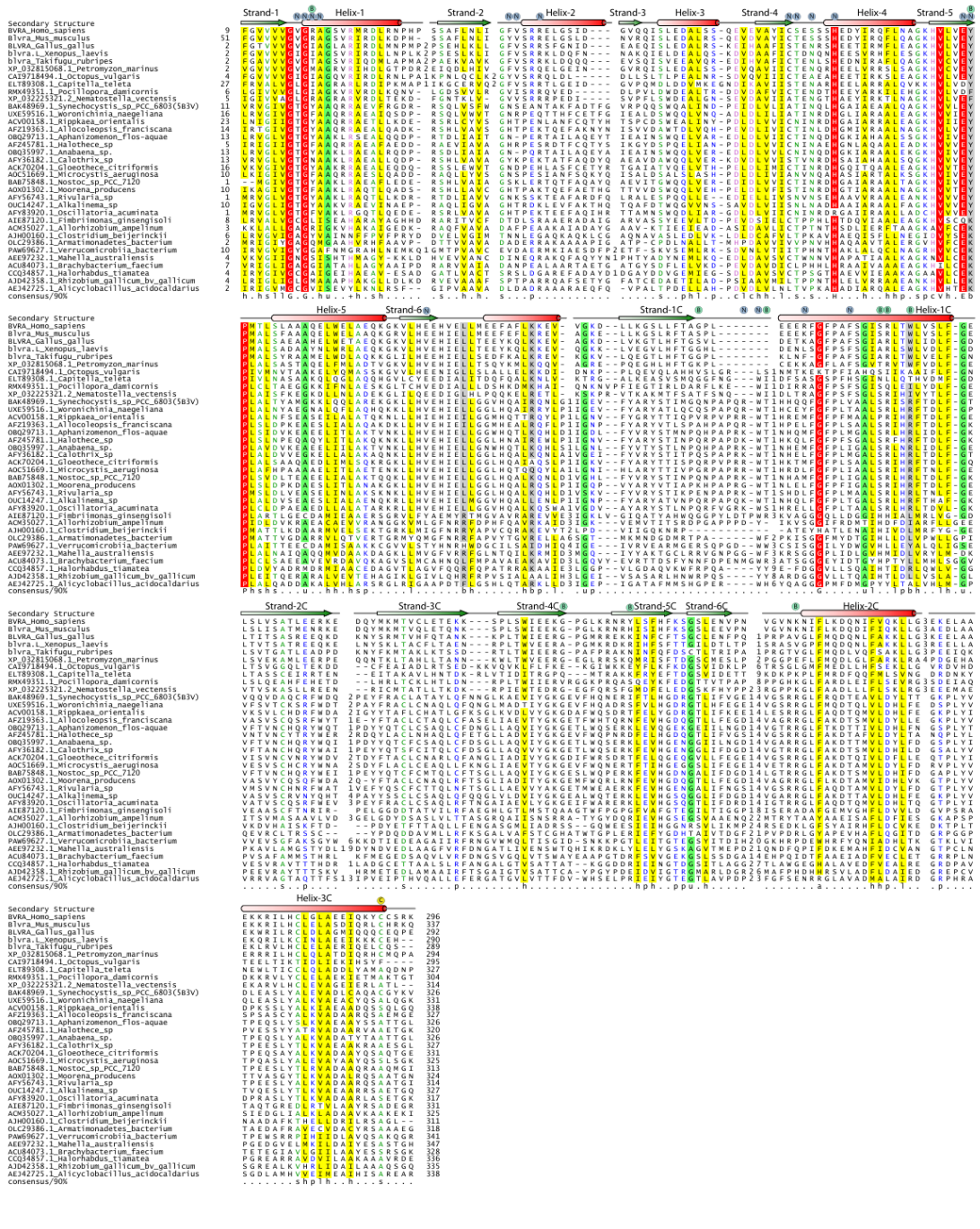

Fig. S1. Domains in BVRA and alignment of BVRA from various species reveals conserved residues in the NAD(P)H and biliverdin binding sites. Multiple sequence alignment of BVRA homologs from eukaryotes to bacteria. Proteins are labeled by their gene names or accession numbers and species names. Secondary structure is provided above the alignment with helices represented by cylinders and strands by arrows. Residue columns are colored by their consensus with absolutely conserved residues shaded red, h (hydrophobic), l (aliphatic), and a (aromatic) residues shaded in yellow; p (polar) residues shown in blue; c (charged) and + (basic) residues are shown in pink font; s (small) is shown in green font; u (tiny) is shown on a green background; and b (big) is shaded gray. The NADPH binding residues (N) and biliverdin binding residues (B) were derived from the structure of the Synechocystis BvrA (pdb: 5B3V). The few additional residues that also bind NADPH in the Rat BVRA (PDB: 1LC0) are also included. C292 of Human BvrA is also indicated.

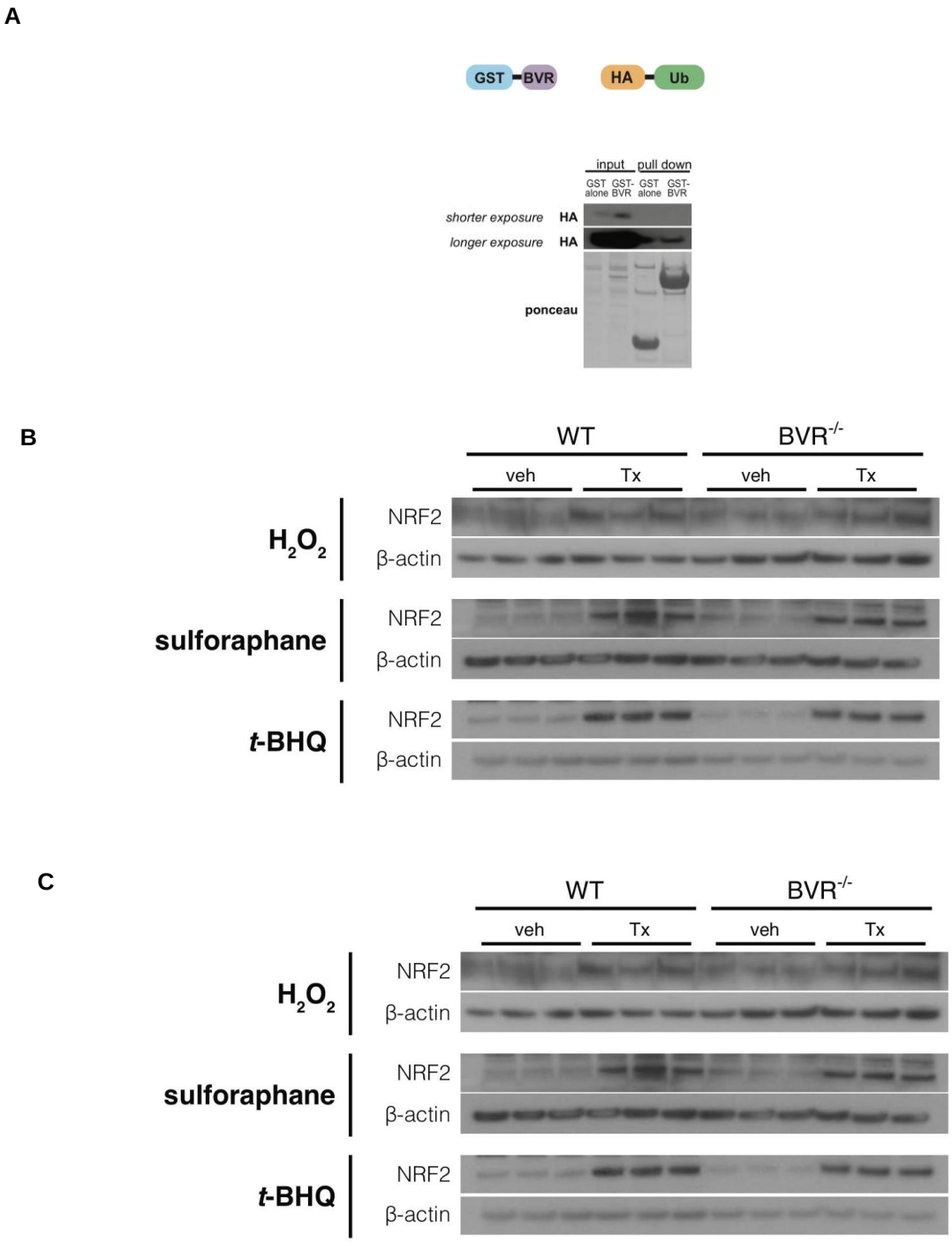

Fig. S2. BVRA does not interact with ubiquitin or modulate either Nrf2 stability or its nuclear translocation. (*A*) BVRA does not interact with Ubiquitin Provide details for each of these. (*B*) Ubiquitination of Nrf2 does not play a role in interaction with BVRA. (*B*) BVRA does not regulate the stability of Nrf2. (*C*) BVRA does not regulate the nuclear localization of Nrf2.

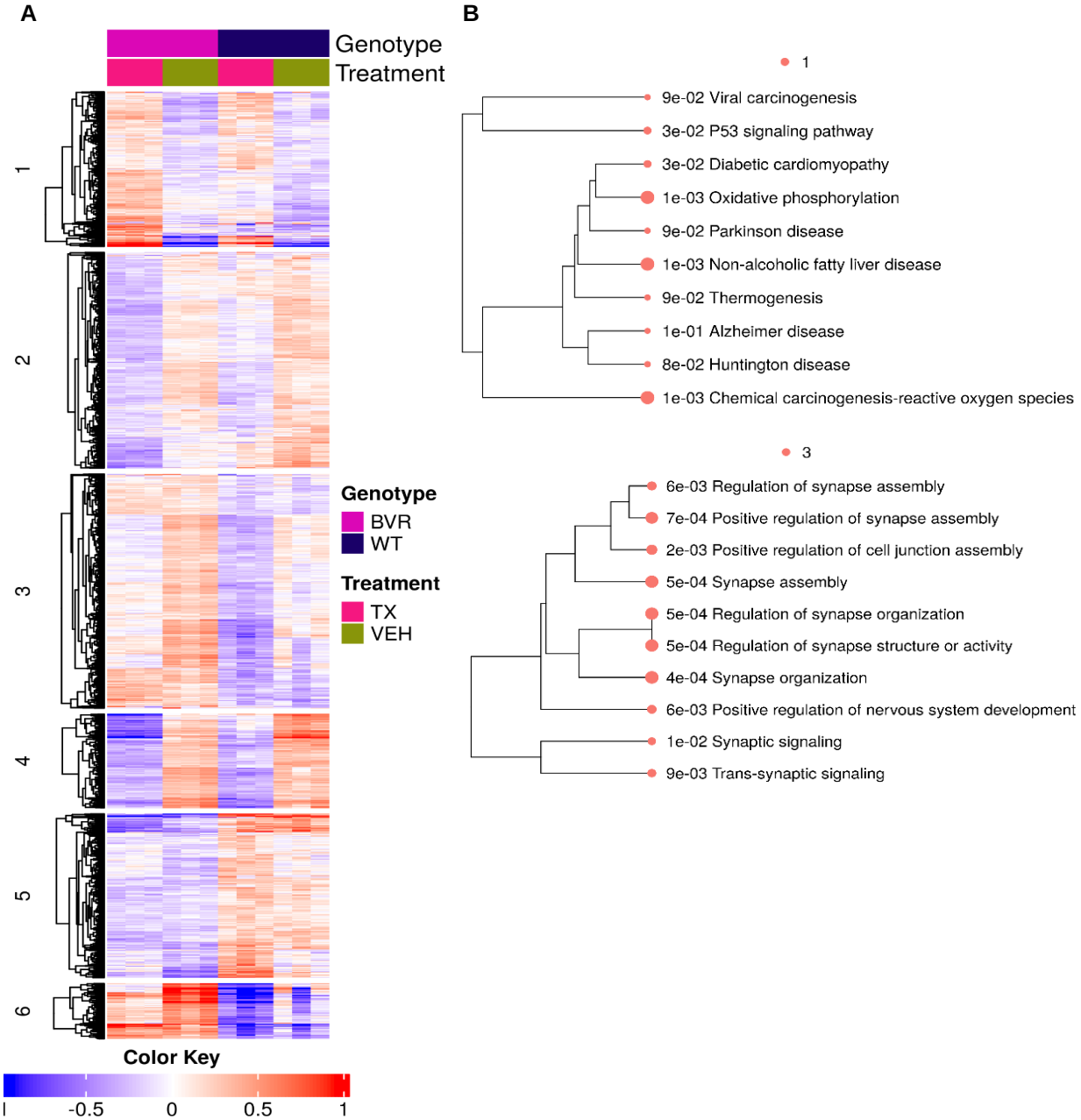

Fig. S3. BVRA Nrf2 coregulated genes are critical in neurophysiology. (*A*) K means clustering of expression of BVRA-Nrf2 associated genes in BVRA and WT (treated with either vehicle (PBS) or H_2O_2. (*B*) Pathway analysis of KEGG on cluster 1 and 3 that shows maximal enrichment with neuronal pathways.

SI References

1. Michaelis L, Menten ML, Johnson KA, & Goody RS (2011) The original Michaelis constant: translation of the 1913 Michaelis-Menten paper. *Biochemistry* 50(39):8264-8269.
2. Dhindsa RS, Zoghbi AW, Krizay DK, Vasavda C, & Goldstein DB (2021) A Transcriptome-Based Drug Discovery Paradigm for Neurodevelopmental Disorders. *Ann Neurol* 89(2):199-211.
3. Paul BD*, et al.* (2014) Cystathionine gamma-lyase deficiency mediates neurodegeneration in Huntington's disease. *Nature* 509(7498):96-100.
4. Sharma SM*, et al.* (2007) MITF and PU.1 recruit p38 MAPK and NFATc1 to target genes during osteoclast differentiation. *J Biol Chem* 282(21):15921-15929.
5. Langmead B, Trapnell C, Pop M, & Salzberg SL (2009) Ultrafast and memory-efficient alignment of short DNA sequences to the human genome. *Genome Biol* 10(3):R25.
6. Heinz S*, et al.* (2010) Simple combinations of lineage-determining transcription factors prime cis-regulatory elements required for macrophage and B cell identities. *Mol Cell* 38(4):576-589.
7. Yu G, Wang LG, & He QY (2015) ChIPseeker: an R/Bioconductor package for ChIP peak annotation, comparison and visualization. *Bioinformatics* 31(14):2382-2383.
8. Altschul SF*, et al.* (1997) Gapped BLAST and PSI-BLAST: a new generation of protein database search programs. *Nucleic Acids Res* 25(17):3389-3402.
9. Lassmann T, Frings O, & Sonnhammer EL (2009) Kalign2: high-performance multiple alignment of protein and nucleotide sequences allowing external features. *Nucleic Acids Res* 37(3):858-865.
10. Katoh K & Standley DM (2013) MAFFT multiple sequence alignment software version 7: improvements in performance and usability. *Mol Biol Evol* 30(4):772-780.
11. Price MN, Dehal PS, & Arkin AP (2010) FastTree 2--approximately maximum-likelihood trees for large alignments. *PLoS One* 5(3):e9490.
12. Sehnal D*, et al.* (2021) Mol* Viewer: modern web app for 3D visualization and analysis of large biomolecular structures. *Nucleic Acids Res* 49(W1):W431-W437.
13. Abramson J*, et al.* (2024) Accurate structure prediction of biomolecular interactions with AlphaFold 3. *Nature* 630(8016):493-500.